SAND2017-2473C

Damage Evolution in 304L Stainless Steel Partial Penetration Laser Welds

Sharlotte Kramer, Amanda Jones, John Emery, and Kyle Karlson
Sandia National Laboratories
1515 Eubank Blvd. SE, Albuquerque, NM 87123

Abstract

Partial penetration laser welds join metal surfaces without additional filler material, providing hermetic seals for a variety of components. The crack-like geometry of a partial penetration weld is a local stress riser that may lead to failure of the component in the weld. Computational modeling of laser welds has shown that the model should include damage evolution to predict the large deformation and failure. We have performed interrupted tensile experiments both to characterize the damage evolution and failure in laser welds and to aid computational modeling of these welds. Several EDM-notched and laser-welded 304L stainless steel tensile coupons were pulled in tension, each one to a different load level, and then sectioned and imaged to show the evolution of damage in the laser weld and in the EDM-notched parent 304L material (having a similar geometry to the partial penetration laser-welded material). SEM imaging of these specimens revealed considerable cracking at the root of the laser welds and some visible micro-cracking in the root of the EDM notch even before peak load was achieved in these specimens. The images also showed deformation-induced damage in the root of the notch and laser weld prior to the appearance of the main crack, though the laser-welded specimens tended to have more extensive damage than the notched material. These experiments show that the local geometry alone is not the cause of the damage, but also microstructure of the laser weld, which requires additional investigation.

Keywords: damage evolution; ductile fracture; laser weld; computational modeling; void nucleation

Introduction

Laser welds are a type of joint formed by the melting of two metals at a seam with a high-powered laser. Oftentimes these welds do not fully penetrate the thickness of the material to prevent damage to nearby heat-sensitive material [1]. These partial penetration laser welds have a crack-like geometry with a local stress riser, leading to failure in the weld of a component under loading. In this study, we consider 304L stainless steel (SS) partial penetration laser welds; Fig.1a is a cross-section of a typical butt-type laser weld in this study with approximately 0.75-mm depth in a 1.55-mm thick sheet. 304L SS is a highly ductile metal, leading to questions of whether the deformation damage mechanisms at the root of the laser weld are dominated by plastic deformation, ductile rupture, void nucleation and growth, or growth of pre-existing pores from the welding process. Previous research has considered deformation of laser welds with the unwelded ligament removed to exclude the stress riser in an initially partial penetration laser weld in 304L SS [2,3] and quantified the variations in weld root porosity [4,5], but this is the first experimental study to systematically characterize damage evolution in these laser welds with the full partial penetration geometry. A computational study of laser weld deformation, based on limited experimental tensile data, combined the material and geometric effects into a surrogate model to represent the laser weld deformation for a component-level analysis with some success [6]. Due to the pragmatic approach of this research, the details of different damage mechanisms were neglected. A different computational study considered the effect of porosity on deformation in laser welds with the unwelded ligament removed [3]. Recent computational efforts in conjunction with this study, with higher-fidelity modeling of full partial penetration laser weld geometry, have highlighted many of the unknowns of the damage evolution. Computational modeling of tensile loading of the local geometry of the laser weld, based on material model calibration of the tensile tests of the base material, cannot predict the early load-drop in the load-displacement behavior of the laser weld geometry. This implies that damage mechanisms based purely on the ductile rupture of the base 304L are insufficient to characterize the damage evolution of these laser welds. Experimental evidence of the damage mechanisms is required to guide improvements in these computational models. In this study, we performed interrupted tensile tests of laser-welded 304L SS to interrogate the local deformation and damage mechanisms in the laser weld. Additionally, we performed interrupted tensile tests of EDM-notched 304L SS specimens (see Fig. 1b), which have a similar pre-notch depth as the unwelded ligament of the laser-welded specimens, though not the same sharp notch tip, to compare the

effect of the local geometry without the complications of the pre-existing porosity, heat affected zone, or change in grain structure in the laser weld as compared to the parent material. In this paper, we detail the experimental methodology of the interrupted testing and post-test measurements of damage, present the experimental results, discuss potential competing damage mechanisms, and identify future areas of research based on these initial findings.

Methodology

The base material in this study was 304L SS sheet material, approximately 1.55-mm thick. Pairs of 76.2-mm x 101.6-mm plates were joined along the long edge with a single laser butt weld. These plates were cut into tensile coupons such that the laser weld was perpendicular to the tensile loading direction. In this study, the rolling direction of the parent 304L SS sheet material was along the short edge of the original plates, meaning the rolling direction of the material was in the direction of the global tensile load of the laser welded specimens. The notched tensile specimens were cut from EDM-notched plates (152.4-mm x 101.6-mm) of the 304L SS with the rolling direction along the tensile direction; the EDM notch was cut in the center of the plate with a nominally 0.2-mm wide EDM-wire, parallel to the short edge of the plate, resulting in a nominally 0.24-mm wide notch with a depth approximately half the thickness of the parent plate. All specimens had a nominal gage width of 6.35-mm.

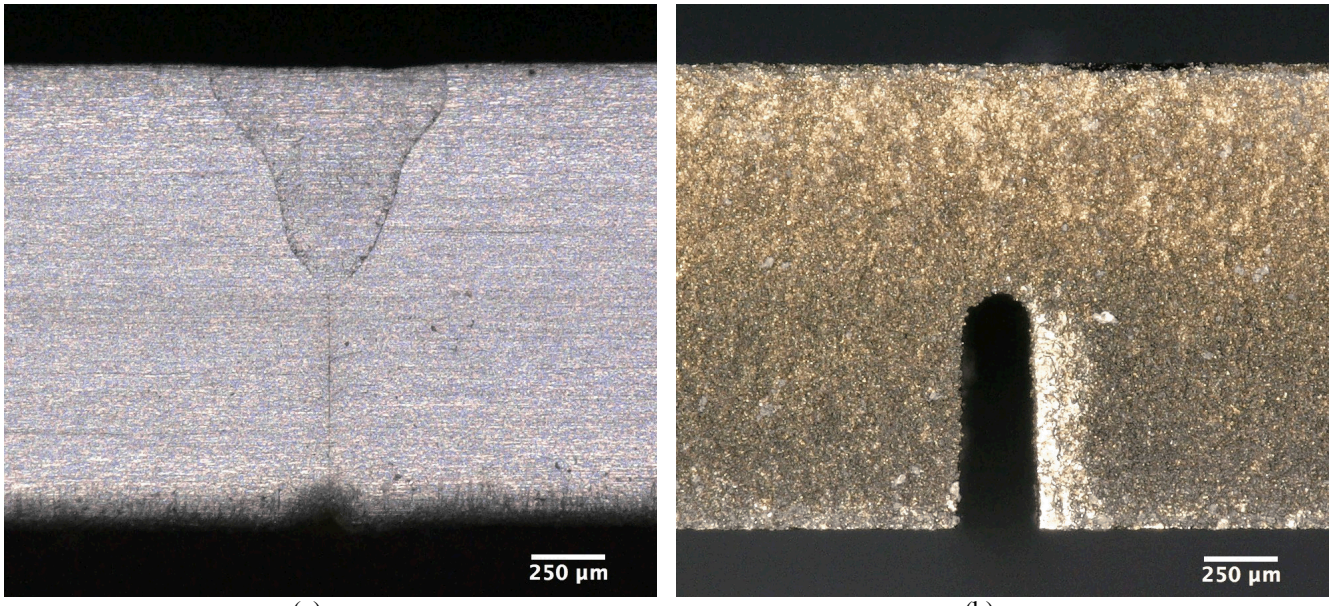

(a) (b)

Fig. 1 (a) Cross-section of a 0.763-mm deep partial penetration laser weld in 1.532-mm thick 304L SS sheet with the laser weld having a keyhole shape and an unwelded ligament (the vertical line below the laser weld); (b) Cross-section of an EDM-notched 304L SS sheet with 0.236-mm notch width and a 0.789-mm notch depth that is similar to the unwelded ligament in the laser welded specimens

We performed base material tensile tests on a custom servo-hydraulic load frame with dual, horizontal, in-line actuators, allowing the center of the specimen to be stationary, which was useful for *in situ* imaging of the local geometry of the notched and welded specimens during the interrupted tensile testing. The specimens were oriented with the width of the specimens along the vertical axis. The global displacement for the base material, notched, and laser welded 304L SS specimens was measured using a 25.4-mm gage length extensometer, attached on the thin side of the specimens; the extensometer body hung vertically below the specimen. Fig. 2 shows the experimental setup, including the Navitar 6000 long-working distance microscope lens and CCD camera that imaged the through-thickness side of the specimens. The base material testing global actuator displacement rate was 12.7 µm/s. The tensile test global actuator displacement rate for the notched and laser welded specimens was 1.27 µm/s or 2.54 µm/s. We tested three base material specimens, one notched specimen to failure, five notched specimens to different displacement / load levels, seven laser-welded specimens to failure, and fourteen laser welded specimens to different displacement / load levels. The notched specimens came from a single notched plate, but the notch depth varied slightly along the plate. The laser-welded specimens came from three different welded plates with slight variations in laser weld depth. The initial interrupted tensile testing focused on loads around peak load for the notched and laser-welded specimens from Plate 4 and 5. Subsequent testing of laser-welded specimens from Plate 6 evenly distributed the tests across the load-displacement curve.

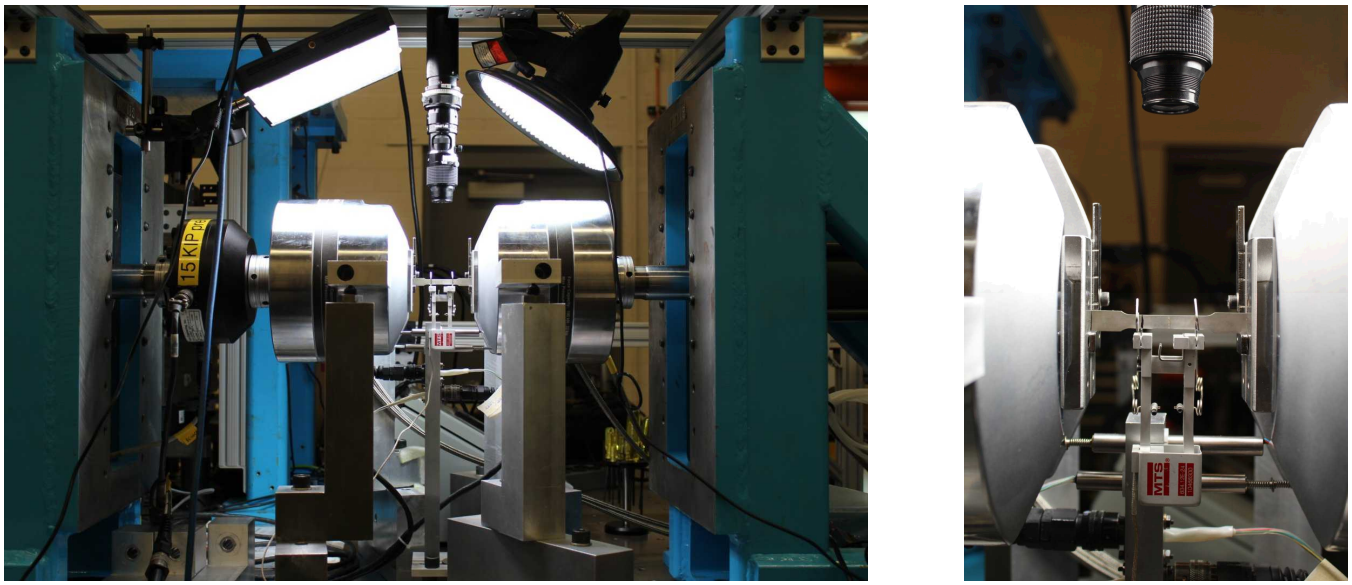

(a) (b)

Fig. 2 Experimental setup for the interrupted tensile testing and base material tensile testing: (a) Custom horizontal, dual-actuator load frame with *in situ* imaging; (b) Close-up view of laser-welded specimen with extensometer and *in situ* imaging

After testing, we imaged the damaged root of the welds and notches using SEM to visualize the damage along the width of the specimens. We also cross-sectioned the deformed specimens along their mid-planes to see the crack growth where there was the highest triaxiality, furthest from the surface. Some of the specimens were etched to see the laser weld structure and the main crack, while others were polished and then SEM imaged in efforts to detect void nucleation.

Results

Fig. 3 shows the engineering stress-strain plot for the base material 304L SS, which had a modulus of 197 GPa, 0.2% offset yield stress of 309 MPa, and ultimate strength of 672 MPa. For the 25.4-mm gage length, nominally 6.35-mm gage width, and 1.55-mm thickness, the failure strain was 72% on average.

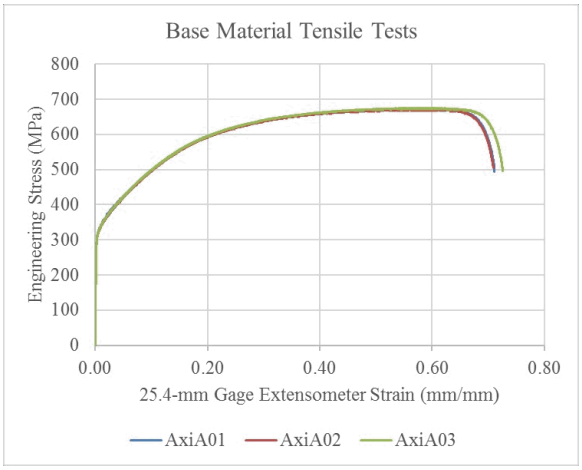

Fig. 3 Engineering stress-strain for three base material 304L SS tensile specimens

The average normalized 25.4-mm gage extensometer displacements to failure for laser-welded Plates 4-6 (only one failure specimen for Plate 6) were 0.052 mm/mm, 0.044 mm/mm, and 0.046 mm/mm, respectively. The material above the notched specimens was on average 0.747 mm deep, in between the weld depths of Plates 5 and 6. The normalized 25.4-mm gage extensometer displacement to failure of the notched specimen was 0.058 mm/mm. Dividing the normalized 25.4-mm gage extensometer displacement of each interrupted test specimen by the normalized 25.4-mm gage extensometer displacement to failure of the parent plate allows us to compare the relative percent displacement to failure of each specimen.

The six notched specimen tension tests, whose load versus normalized extensometer displacement plots are shown in Fig. 4a, had different load goals and corresponding percent displacements to failure: 98% of the estimated peak load before peak, 52% displacement to failure; peak load, 74% displacement to failure; a repeat of peak load, 81% displacement to failure; 97% of peak load after peak load, 67% displacement to failure; 90% of peak load after peak load, 85% displacement to failure; and complete failure. Fig. 4b-d show the load vs. normalized extensometer displacement plots for the laser-welded specimens from Plates 4-6, respectively. The load goals and corresponding percent displacements to failure for the eight specimens from Plate 4 were 98% of the estimated peak load before peak, 63% displacement to failure; 99% of the estimated peak load before peak, 66% displacement to failure; peak load, 79% displacement to failure; a repeat of peak load, 77% displacement to failure; 98% of peak load after peak load, 82% displacement to failure; and three specimens to complete failure. The load goals and corresponding percent displacements to failure for the eight specimens from Plate 5 were peak load, 73% displacement to failure; a repeat of peak load, 77% displacement to failure; 98% of peak load after peak load, 79% displacement to failure; 95% of peak load after peak load, 84% displacement to failure; 90% of peak load after peak load, 82% displacement to failure; and three specimens to complete failure. The load goals and corresponding percent displacements to failure for the five specimens from Plate 6 were immediately unloaded after the initial slope change in the load-displacement curve (colloquially called "post-yield" at 76% of the estimated peak load before peak), 11% displacement to failure; one third between the initial slope change and peak load (colloquially called "1/3 of hardening" at 87% of the estimated peak load before peak), 26% displacement to failure; two thirds between the initial slope change and peak load (colloquially called "2/3 of hardening" at 96% of the estimated peak load before peak), 42% displacement to failure; peak load, 60% displacement to failure; and complete failure. Plate 4 had the deepest welds with an average of 0.794 mm; Plate 5 had an average weld depth of 0.757 mm; and Plate 6 had an average weld depth of 0.737 mm. The variation in the displacement to failure for the laser-welded specimens is likely due to weld penetration depth, where the deeper the weld, the longer the displacement to failure.

Fig. 5 includes central cross-sections of six laser-welded specimens with increasing levels of deformation. These cross-sections, which have been etched to relieve the laser welds, show an increase in crack length with increased deformation. Notably in Fig. 5a, a small crack does appear after the initial change in slope of the global load-displacement curve. The crack growth dramatically increases before peak load and afterwards. Fig. 6 has SEM images of polished central cross-sections of notched and laser-specimens with load levels just before and after peak load. The notched specimens show considerable deformation in the curved portion of the notch, but the presence of cracks is not clear before peak load from this view. In contrast, the crack growth into laser welds is apparent in both laser-welded specimens. All four of these specimens show evidence of void nucleation ahead of the free surface in the electron backscatter diffraction (EBSD) SEM view of the root of the notch / crack tip. Fig. 7 includes SEM images of the root of the notch or laser weld from the perspective of the advancing deformation / crack; these images were taken prior to sectioning and view the central portion of the root of the notch or laser weld. Fig. 7a-b shows the roots of the notches of the 98% peak load (before estimated peak load) and 90% peak load (after peak load) specimens, which are the same as those in Fig. 6a-b. Fig. 7a clearly shows horizontal cracks at the root of the notch; higher magnification images (not provided here) show micro-scale cracking as well. Fig. 7b shows the crack more prominently at the root of the notch. Fig. 7c-f shows the damage and crack propagation of laser-welded specimens with increasing global deformation [note: the image magnification changes with each successive level of deformation.] Fig. 7c has clear evidence of ductile rupture and horizontal cracks for the least global deformation level, just beyond the slope change of the load-displacement curve; also the preexisting pores from the welding process are deforming and are cracking open, seen as the vertically elongated oval structure in the root of the weld. Fig. 7d-f shows evidence of extensive plastic deformation, ductile rupture, and pore deformation and coalescence with the main crack.

Discussion and Future Work

The initial hypothesis used in the computational modeling of these notched and laser-welded geometries of 304L SS was that the global load-displacement curve behavior was dominated by extensive plastic deformation and necking processes of the highly ductile 304L SS base material [6]. In contrast, this experimental study has shown that damage and crack propagation occur much earlier, just after the initial slope change of the global load-displacement curve, progress steadily through the next slope of the global load-displacement curve, and then quickly advances between peak load to failure. This observed behavior is similar to that of a single edge-notched tension (SENT) geometry specimen, but without a fatigue pre-crack; tensile loading of a SENT geometry in a ductile material can provide a J resistance curve [7]. The initial slope-change of the load-displacement curve is potentially due to the local crack growth at the root of the laser weld and not just material yielding and hardening; further research is needed to determine if the blunt notch produces the same crack growth behavior upon the initial slope change of the load-displacement curve. Nevertheless, both the notched and laser-welded specimens have considerable crack damage and void nucleation ahead of the crack tip prior to peak load of the structures.

The damage is more pronounced in the case of the laser welds as compared to the notched specimens because of the sharper notch at the root of the weld acting as a larger stress concentration as well as preexisting pores at the root of the weld. The size and distribution of these preexisting pores are yet unknown for this particular weld, but these welds have pores that can greatly vary in size from those that can be detected with micro-computed tomography (CT) on the order of 10-μm and larger [4,5] down to smaller pores only measured through destructive sectioning and imaging of undeformed welds. A few specimens of this particular laser weld were imaged with micro-CT, showing only on the order of three to five large-scale pores over each 6.35-mm specimen width. The deformed and cracked pores in the root of the least deformed laser-welded specimen in Fig. 7c were likely smaller than could be detected by micro-CT. The roots of these laser-welded specimens show evidence of extensive pore growth, deformation, and cracking in several pores that were originally small, probably less than 10-μm. In contrast, the roots of the notched specimens mostly show the horizontal cracking and micro-cracks. We do not know the influence of the EDM oxide-layer surface finish on the initiation of the cracks early in the deformation, but the extensive horizontal cracks and micro-cracks after large global deformation are visible in the underlying deformed 304L SS. These same types of cracks are evident in the laser welds in locations away from the pores, so this damage is probably from the geometry, not surface effects. The void nucleation ahead of the main cracks is found in the cross-sections of both the notched and laser-welded specimens. This may be the main crack damage mechanism in the notched specimens, but the damage evolution in laser-welded specimens is more complex with the preexisting pores, void nucleation, and variation in laser weld penetration depth along the width of the specimen.

This study leads to several research opportunities to elucidate these damage mechanisms. Additional interrupted tests of notched specimens, including lower levels of deformation, could determine when cracks begin to form in the notched specimens, which, when compared to the laser-welded specimens, could determine if the native pores or void nucleation is the predominant damage mechanism at the onset of damage. Not all central cross-sections of the specimens have been polished and SEM imaged; these images of the lower deformation laser-welded specimens may also help to determine if the pores or void nucleation is the predominant damage mechanism at the onset of damage. EBSD of the deformed and undeformed notched and laser welded specimens would provide data on grain structure and evolution of plastic deformation ahead of the damage, perhaps revealing the true role of plastic deformation in these geometries. Destructive sectioning and imaging of undeformed laser-welded specimens could quantify the distribution of preexisting pores in these welds, which we suspect are a driving factor in the extensive early damage in these structures.

Summary

This study has considered the damage evolution in notched and partial-penetration, laser-welded tensile specimens of 304L SS. The experimental approach of interrupting the tensile tests at various levels of deformation and imaging the deformed specimens has allowed us to refute a previously held assumption that these structures are dominated by plastic deformation rather than damage at the stress concentrations of these geometries. The data clearly shows early crack damage with steady growth before peak tensile load of these specimens. Notched and laser-welded specimens both have crack damage prior to peak tensile load. Further research is necessary to clarify the roles of the geometry, preexisting pores in the laser weld, plastic deformation, and void nucleation have on the damage mechanisms in these structures.

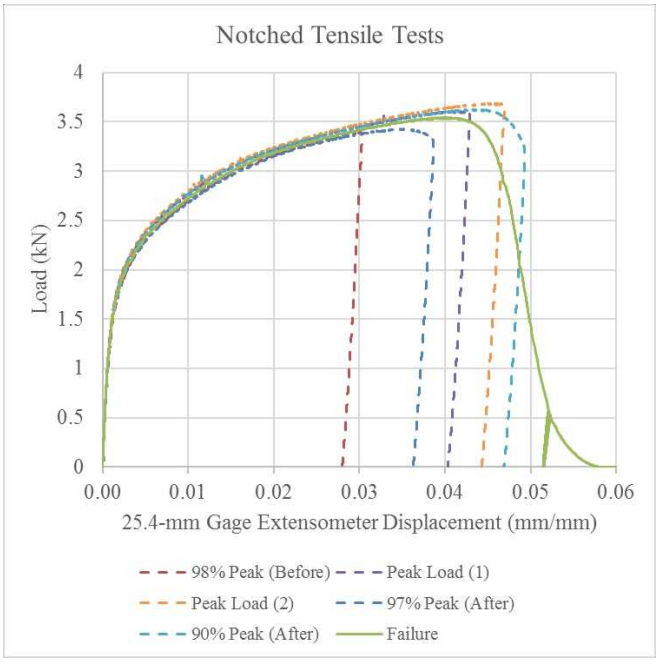

(a)

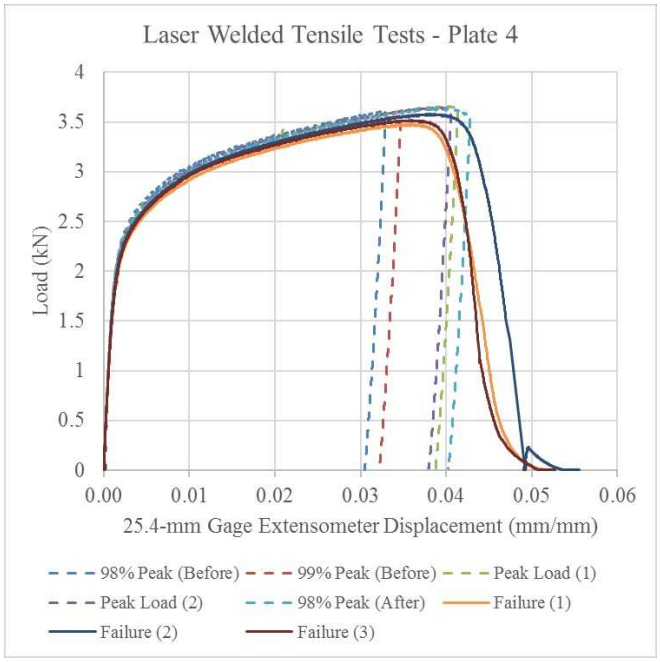

(b)

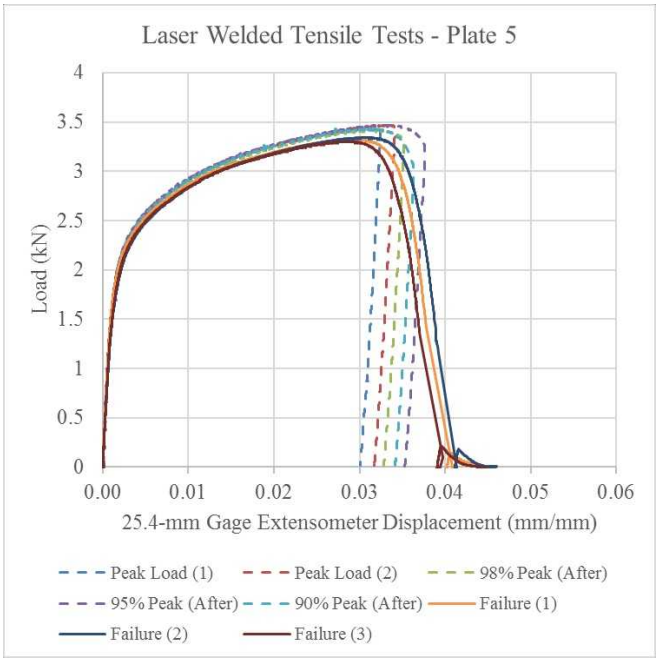

(c)

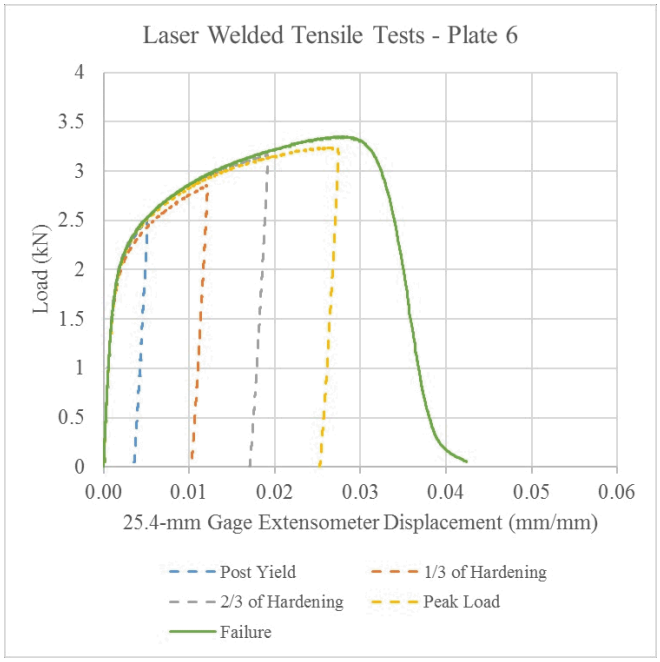

(d)

Fig. 4 Experimental data from interrupted tensile testing: (a) load vs. extensometer normalized displacement for notched specimens; (b) load vs. extensometer normalized displacement for Plate 4 of the laser-welded specimens; (c) load vs. extensometer normalized displacement for Plate 5 of the laser-welded specimens; and (d) load vs. extensometer normalized displacement for Plate 6 of the laser-welded specimens

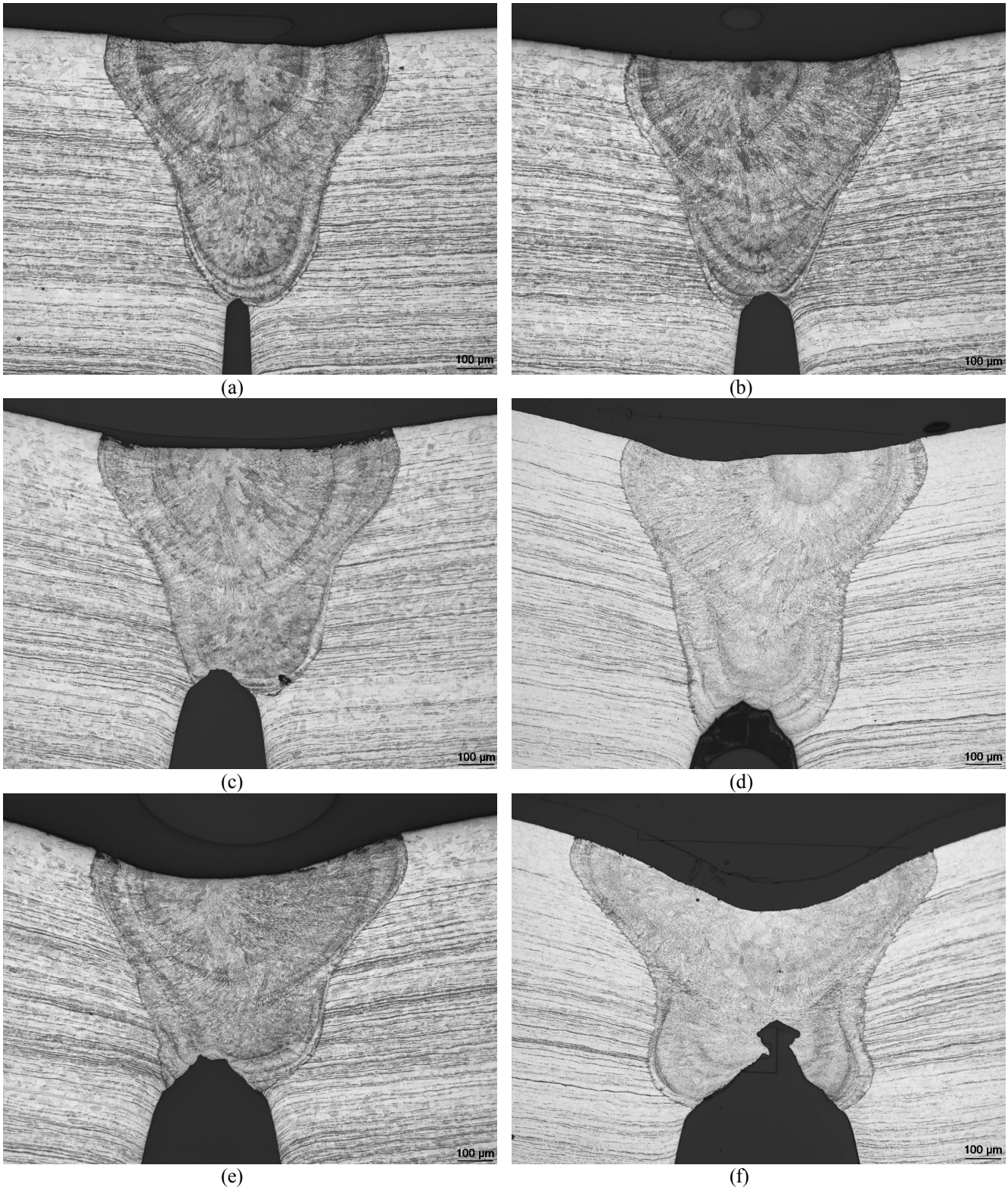

(a) (b)

(c) (d)

(e) (f)

Fig. 5 Etched central cross-sections from select laser-welded specimens, showing increased crack growth as displacement increased: (a) Plate 6 "post-yield" specimen, 11% displacement to failure; (b) Plate 6 "1/3 of hardening" specimen, 26% displacement to failure; (c) Plate 6 "2/3 of hardening" specimen, 42% displacement to failure; (d) Plate 4 98% peak-load (before estimated peak load) specimen, 63% displacement to failure; (e) Plate 6 peak-load specimen, 60% displacement to failure; and (f) Plate 5 90% peak-load (after peak load) specimen, 82% displacement to failure

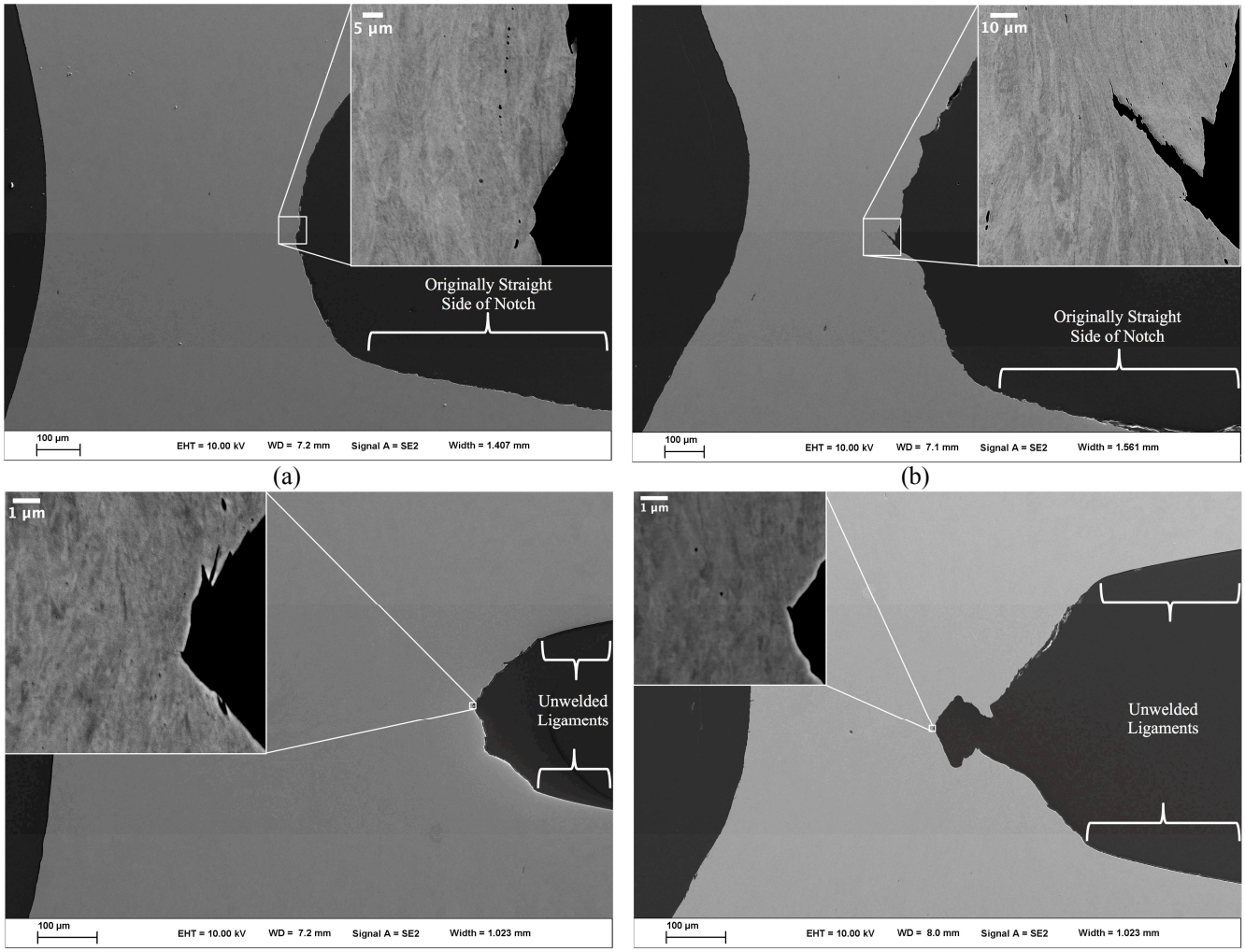

Fig. 6 Polished cross-sections from select notched and laser-welded specimens (oriented 90-degrees and inverted from corresponding Fig. 5 images), with inset electron backscatter diffraction SEM images near the crack tip to show void nucleation: (a) notched 98% peak-load (before estimated peak load) specimen, 52% displacement to failure; (b) notched 90% peak-load (after peak load) specimen, 85% displacement to failure; (c) Plate 4 98% peak-load (before estimated peak load) specimen, 63% displacement to failure; and (d) Plate 5 90% peak-load (after peak load) specimen, 82% displacement to failure

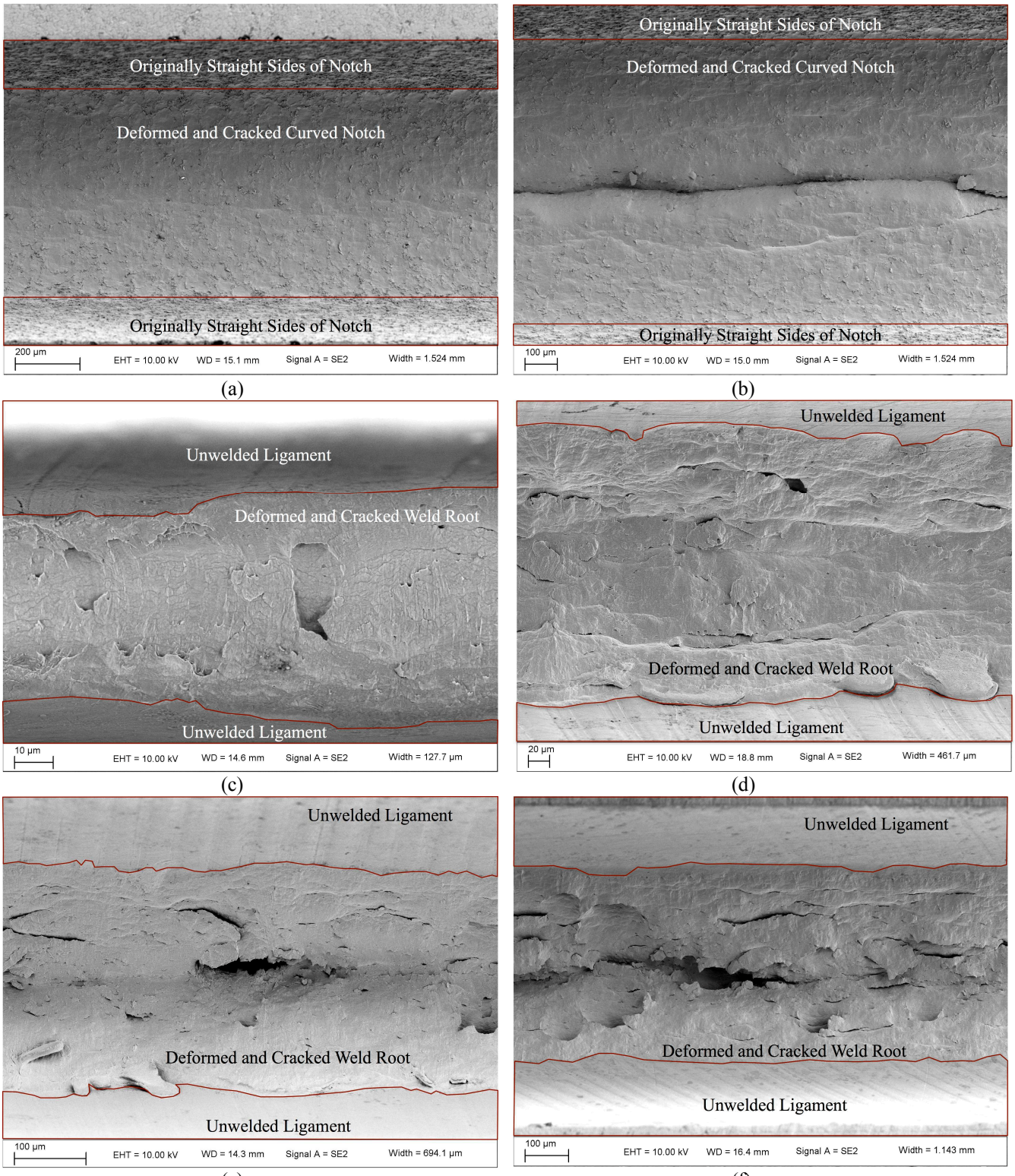

Fig. 7 SEM images of the root of select notched and laser welded specimens: (a) notched 98% peak-load (before estimated peak load) specimen, 52% displacement to failure; (b) notched 90% peak-load (after peak load) specimen, 85% displacement to failure; (c) Plate 6 “post-yield” specimen, 11% displacement to failure; (d) Plate 4 98% peak-load (before estimated peak load) specimen, 63% displacement to failure; (e) Plate 6 peak-load specimen, 60% displacement to failure; and (f) Plate 5 90% peak-load (after peak load) specimen, 82% displacement to failure

References

[1] Miyamoto I, Knorovsky GA. Laser micro welding. In *Microjoining and Nanojoining*, Zhou Y (ed.). Woodhead Publishing Limited: Abington Hall, Abington, Cambridge, CB21 6AH, England; 345–417, 2008.

[2] Boyce BL, Reu PL, Robino CV. The constitutive behavior of laser welds in 304l stainless steel determined by digital image correlation. *Metallurgical and Materials Transactions A.* 37A, 2481–2492, 2006.

[3] Madison, J. D., Aagesen, L. K., Battaile, C. C., Rodelas, J. M., & Payton, T. K. C. S. (2013). Coupling 3D Quantitative Interrogation of Weld Microstructure with 3D Models of Mechanical Response. *Metallography, Microstructure and Analysis,* 2(6), 359-363, 2013

[4] Madison JD, Aagesen LK. Quantitative characterization of porosity in laser welds of stainless steel. *Scripta Materialia* 67, 783–786, 2012.

[5] Madison, J., Aagesen, L. K., Chan, V. W. L., & Thornton, K. Advancing Quantitative Description of Porosity in Autogenous Laser-Welds of 304L Stainless Steel. *Integrating Materials and Manufacturing Innovation, 3*(11), 2014.

[6] Emery,J.M., Field, Jr., R.V., Foulk, III, J.W., Karlson, K.N., and Grigoriu, M., Predicting laser weld reliability with stochastic reduced-order models. *International Journal for Numerical Methods in Engineering*, 103, 914-936, 2015.

[7] Anderson, T.L. *Fracture Mechanics: Fundamentals and Applications*. (3rd ed.) CRC Press: Boca Raton, FL; 114-128, 2005.

Acknowledgements

We would like to thank B. Boyce and J. Carroll for discussions regarding the experiments; B. McKenzie for the SEM imaging; D. MacCallum, D. Johnson, C. McConnell, and D. Pendley for specimen preparation; and A. Kilgo and C. Profazi for sectioning and imaging the specimens.

Sandia National Laboratories is a multi-program laboratory managed and operated by Sandia Corporation, a wholly owned subsidiary of Lockheed Martin Corporation, for the U.S. Department of Energy's National Nuclear Security Administration under contract DE-AC04-94AL85000.